

Oxidation-Induced Deep Levels in *n*- and *p*-Type 4H- and 6H-SiC and Their Influence on Carrier Lifetime

I. D. Booker,^{*} H. Abdalla, J. Hassan, R. Karhu, L. Lilja, and E. Janzén[†]

Department of Physics, Chemistry and Biology (IFM), Semiconductor Materials Division, Linköping University, 581 83 Linköping, Sweden

E. Ö. Sveinbjörnsson[‡]

Department of Physics, Chemistry and Biology (IFM), Semiconductor Materials Division, Linköping University, 581 83 Linköping, Sweden and Science Institute, University of Iceland, IS-107, Reykjavik, Iceland

(Received 8 March 2016; published 19 July 2016)

We present a complete analysis of the electron- and hole-capture and -emission processes of the deep levels ON1, ON2a, and ON2b in 4H-SiC and their 6H-SiC counterparts OS1a and OS1b through OS3a and OS3b, which are produced by lifetime enhancement oxidation or implantation and annealing techniques. The modeling is based on a simultaneous numerical fitting of multiple high-resolution capacitance deep-level transient spectroscopy spectra measured with different filling-pulse lengths in *n*- and *p*-type material. All defects are found to be double-donor-type positive-*U* two-level defects with very small hole-capture cross sections, making them recombination centers of low efficiency, in accordance with minority-carrier-lifetime measurements. Their behavior as trapping and weak recombination centers, their large concentrations resulting from the lifetime enhancement oxidations, and their high thermal stability, however, make it advisable to minimize their presence in active regions of devices, for example, the base layer of bipolar junction transistors.

DOI: 10.1103/PhysRevApplied.6.014010

I. INTRODUCTION

The increasing target application voltages of 4H-SiC bipolar devices such as insulated-gate bipolar transistors demand that the carrier lifetime in the thick low-doped drift layer of the device needs also to be increased to allow for optimal conductivity modulation. The main point-defect recombination centers in 4H-SiC which limit this development have been identified as the carbon-vacancy- (V_C) related $Z_{1/2}$ deep levels, made up of two negative-*U* two-level defects on the *h* and *k* inequivalent lattice sites [1,2]. In 6H-SiC, three similar negative-*U* defects can be found in deep-level transient spectroscopy (DLTS) spectra, which are referred to as $E1/E2$ and are also thought to be related to V_C on the three inequivalent lattice sites [3–5]. One method to remove V_C -based deep levels in 4H-SiC and improve the epilayer carrier lifetime is thermal oxidation, where excess carbon interstitials (C_i) generated at the SiO_2/SiC interface diffuse into the epilayer and recombine with or disable the V_C deep levels [6]. To improve the carrier lifetime throughout the entire *n*- or *p*-type epilayer thickness, which can be 100 μm or greater for very-high-voltage devices, oxidations at temperatures from 1300 to 1500 $^\circ\text{C}$ for up to several tens of hours are required. The

high-temperature oxidation of *n*-type 4H-SiC is found to create a number of new deep levels in large concentrations in the top half of the band gap which are referred to as ON1, ON2a/b [7]. These levels are highly stable and persist up to annealing temperatures around 1800 $^\circ\text{C}$ [8]. In *p*-type 4H-SiC, oxidations at 1300 $^\circ\text{C}$ are found to produce the HK0 deep level in the lower half of the band gap, which, however, could easily be removed by annealing the samples at 1400 $^\circ\text{C}$ [9]. In some samples, additional deep levels, also unstable against high-temperature annealing, could also be detected [10]. In this paper, we present a complete analysis of the electrical properties of the oxidation-induced deep levels in the upper half of the band gap of *n*- and *p*-type 4H- and 6H-SiC. By using capacitance transient spectroscopy with different combinations of electrical and optical filling and emptying pulses, we show that the three discernable 4H-SiC DLTS peaks are the product of two positive-*U*, double-donor-type defects, while the six discernable peaks in 6H-SiC appear to be the result of three positive-*U* double-donor-type defects. The defects are shown to be recombination centers of far lower efficiency than V_C and influence charge-carrier lifetimes only when they occur in large concentrations, which is the case in the first several micrometers of semiconductor material adjacent to the oxidized surface [11]. The semiconductor surface used for the lifetime enhancement oxidation must therefore be chosen carefully. Their presence should be minimized, for example, in the thin, current-carrying base

^{*}ianbo@ifm.liu.se

[†]erija@ifm.liu.se

[‡]einars@hi.is

layers of bipolar junction transistors while it is expected to be of lesser concern in the thick drift layers. While not yet investigated, a detrimental effect on the threshold voltage and inversion channel mobility of unipolar metal-oxide-semiconductor field-effect transistors may also occur due to charge-carrier trapping and scattering.

II. EXPERIMENTAL METHODS

4H-SiC and *6H-SiC* epilayers are grown in four different horizontal and vertical hot-wall reactors on highly doped substrates of their respective polytypes [12]. Aluminum is used for *p*-type doping in the 1×10^{15} – $1 \times 10^{16} \text{ cm}^{-3}$ range, while nitrogen is used in the growth of 5×10^{14} – $1 \times 10^{16} \text{ cm}^{-3}$ doped *n*-type samples. The *4H-SiC* sample epilayer thicknesses are 50 μm for the *n*-type and 150 μm for the *p*-type material, while the thicknesses of *6H-SiC* epilayers varies from 19 to 25 μm . The samples are then oxidized in a quartz tube reactor using a mixture of Ar and dry O₂ at 800-mbar pressure, with the temperature and duration varying from 1300 to 1500 °C and 300 to 1000 min, respectively.

Round 0.8- to 1.2-mm-diameter Schottky contacts made of 20- or 100-nm-thick Ni or Ti are thermally evaporated onto the epilayers. The semitransparent 20-nm-thick contacts have transmittance values greater than 10% for 355-nm laser light and are stable up to 630 K, allowing optical injection and diffusion of charge carriers into the space-charge region below the contact. Large Ohmic backside contacts are made using Ag paste. For all transient capacitance measurements on the samples, a Boonton 7200 capacitance meter is used. To study majority-carrier capture at majority traps in the top half of the band gap in *n*-type material, DLTS at a reverse bias of –10 V is measured in a temperature range of 77–690 K and transients of up to 10-s length are collected [13]. For filling-pulse measurements, the 10-V filling-pulse widths are varied from 50×10^{-9} to 1×10^{-2} s, allowing a direct measure of the electron-capture cross section (σ_n) and its temperature dependence. The double-DLTS (D-DLTS) and reverse-DLTS (R-DLTS) techniques are used for concentration depth profiling and analysis of the emission-rate field dependence [14,15].

Minority-carrier transient spectroscopy (MCTS) is used to study electron capture by minority traps in the upper half of the *p*-type band gap [16]. A 355-nm Nd:YAG 10-kHz pulsed laser is used to create electron-hole pairs in the space-charge region and in the neutral region below by band-to-band absorption while the reverse bias is kept constant. The majority carriers (holes) are immediately swept out of the space-charge region by the electric field in the time frame of a few tens to hundreds of femtoseconds, while minority carriers (electrons) which diffuse to the edge of the space-charge region are swept in. The result is a minority-carrier density in the space-charge region which exceeds the majority-carrier density, allowing the

measurement of deep levels with $\sigma_n > \sigma_p$ in *p*-type material. The injection level is varied from 1×10^9 to $1 \times 10^{15} \text{ cm}^{-3}$ in the space-charge region while making sure the excess carrier density remains below 10% of the sample doping density. We use two further techniques which we refer to as optical-DLTS (O-DLTS) and optical-electrical-MCTS (OE-MCTS) in this paper. In O-DLTS, an optical carrier injection pulse is used while keeping the reverse bias constant. In contrast to MCTS, however, this measurement is done on *n*-type samples, and we monitor majority (electron) capture by electron traps in the upper half of the band gap. By controlling the laser power, the total number of electrons excited above the band gap into the conduction band and available for capture by hole-repulsive deep levels in the space-charge region can be reduced to levels significantly below those in DLTS using the shortest pulses available with our pulse generator (50×10^{-9} s). For deep levels which are neutral or attractive to holes, the electron capture competes with the capture of the holes present in a significantly higher concentration, which results in reduced or vanishing peak amplitudes. To measure the hole-capture cross sections of minority (electron) traps in the upper half of the *p*-type band gap, we use OE-MCTS. An optical pulse creates an initial electron population on the deep levels which is defined by their ratio of σ_p to σ_n and the density of the available carriers. Directly after the optical pulse, an electrical pulse of length 50×10^{-9} s to 1×10^{-2} s is used to allow hole capture by the deep levels in a field-free environment, giving us a direct measure of σ_p using the filling-pulse technique.

The minority-charge-carrier lifetimes are measured via time-resolved photoluminescence (TRPL) at room temperature using the same pulsed laser as the other techniques with an injection level in the low 10^{16}-cm^{-3} range. A Hamamatsu photomultiplier tube with laser cutoff and bandpass filters is used to collect the near-band-gap luminescence and the transients are recorded by a digital oscilloscope taking 28 000 averages. The dynamic range of the measurements is greater than 4 orders of magnitude, and the minority lifetime is extracted by fitting an exponential function to the low-intensity, asymptotic part of the decay curve.

III. MODELING

The deep levels analyzed in this paper are the product of defects with three possible charge states, doubly positive (2+), singly positive (+), and neutral (0), giving rise to two levels (+|0) and (2+|+) in the band gap. The level occupation after short-duration filling or emptying pulses in DLTS or OE-MCTS, respectively, is thus complicated by an interrelation between the two levels. Our model, described in the following paragraphs, for the medium- and high-resolution multispectra fitting procedure is derived under the assumption of detailed balance and allows competing electron and hole capture to occur into

these two interrelated levels, thus expanding the models available in the literature [17]. Fitting multiple (four or more) spectra made with different filling-pulse lengths simultaneously is necessary to derive meaningful parameters for the thermal activation energies or enthalpies ΔH , entropy factors χ , and the temperature dependencies of the capture cross sections σ_n and σ_p , specifically in our case of strongly overlapping levels. A general advantage of multispectra fitting over the more traditional Arrhenius plot method, which uses only the peak center position as input, is that the entire shape of the peak is included in the analysis of the deep level. Even in the case of the ON1 peak, which appears well separated at first glance, we see that an analysis limited only to the peak center position leads to erroneous conclusions on the nature of the defect and full multispectra fitting is needed. Even more significantly, fitting only a single spectrum with a two-level defect model allows a large number of potential parameter combinations with near-equally good fits. Fitting multiple spectra simultaneously reduces the number of possible parameter combinations, and, after discarding models with unphysical solutions or large sum-square errors, we may reduce our options down to one or two sets of solution parameters for further testing. We also include a numerical approximation of the slow capture and reemission at the edge of the space-charge region during the filling pulse (referred to as the transition region) to expand the range of filling-pulse lengths we can model relative to what is possible using only a simple analytical depletion approximation.

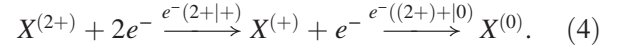
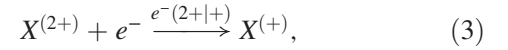
DLTS spectra $S(t)$ are calculated from the capacitance transients $C(t)$, measured at different temperatures for a duration t_c after a short time delay t_d after the filling pulse, by applying a correlation function $W(t)$:

$$S = t_c^{-1} \int_{t_d}^{t_d+t_c} \Delta C(t) W(t) dt. \quad (1)$$

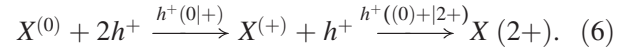
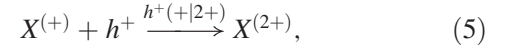
Because medium to high resolution is required, we employ the Gaver-Stehfest 4 (GS4) and 6 (GS6) correlation functions [18]. For deep-level concentrations which are small compared to the doping concentration, the total capacitance transient $\Delta C(t)$ is proportional to the change of the occupied fraction $\Delta f(t)$ of the deep levels:

$$\Delta C(t) \propto - \sum_i^N \Delta f_i(t). \quad (2)$$

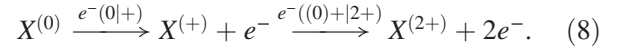
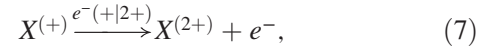
To correctly calculate the electron-occupied fractions of the two-level defect after an electron (DLTS) or hole injection pulse (OE-MCTS) of duration t_p , all possible defect reactions must be taken into account. These are all single electron- and hole-capture and -reemission processes, where the electron-capture reactions are



The first electron is captured into the empty defect $X^{(2+)}$ with a rate c_{n2+} , while the second electron is captured into $X^{(+)}$ at a rate c_{n+} . The analog reactions for hole capture into singly- ($X^{(+)}$) or doubly- ($X^{(0)}$) electron-occupied defects are



The inverse emission processes, which occur during the measurement of the electron emission from the space-charge region or which may be of relevance in the transition region during the filling pulse, are



Hole emission is ignored, as it is negligible for deep levels in the upper half of the band gap. The capture rates in Eqs. (3)–(8), with electron (n) or hole (p) densities and thermal velocities $\langle v_{th(n,p)} \rangle$, may be written as

$$c_{n2+,n+} = \sigma_{n2+,n+}(T) \langle v_{th(n)} \rangle n, \quad (9)$$

$$c_{p+,p0} = \sigma_{p+,p0}(T) \langle v_{th(p)} \rangle p, \quad (10)$$

and the emission rates are [19]

$$e_{n+,n0} = \sigma_{n2+,n+}(T) N_C \langle v_{th(n)} \rangle \chi_{1,2} \exp \frac{-\Delta H_{1,2}}{k_B T}, \quad (11)$$

$$\chi_{1,2} = \frac{g_0}{g_1} \exp \frac{\Delta S_{1,2}}{k_B}, \quad (12)$$

where N_C is the effective density of states in the conduction band and the indices 1 and 2 stand for the (+|2+) and (0|+) transitions, respectively. The defect enthalpy $\Delta H_{1,2}$ and the entropy $\Delta S_{1,2}$, which cannot be separated from the electronic degeneracies g_0 and g_1 [which is 2 and $\frac{1}{2}$ for the (2+|+) and (+|0) transitions, respectively] in the entropy factor $\chi_{1,2}$, can then be used to derive an approximate actual energy separation from the conduction (E_C) or valence band (E_V) given by $\Delta G_{1,2} = \Delta H_{1,2} - T\Delta S_{1,2} = E_C - E_{T1,2}$.

The defect reactions in Eqs. (3)–(8) lead to a set of coupled differential equations describing the development

of the fractions f^+ and f^0 of singly $X^{(+)}$ and doubly $X^{(0)}$ occupied defects during the filling phase:

$$\begin{aligned} \frac{\delta f^+}{\delta t} &= c_{n2+}(1 - f^+ - f^0) - c_{n+}f^+ - c_{p+}f^+ \\ &\quad + c_{p0}f^0 - e_{n+}f^+ + e_{n0}f^0, \end{aligned} \quad (13)$$

$$\frac{\delta f^0}{\delta t} = c_{n+}f^+ - c_{p0}f^0 - e_{n0}f^0. \quad (14)$$

After setting the occupancy after the filling pulse and, again, ignoring the negligible hole-emission rates for defects in the upper half of the band gap, the defect reactions which can occur during electron emission in the measurement time period of length t_c are given by Eqs. (7) and (8). The result is, again, a set of coupled differential equations describing the occupancy evolution during electron emission:

$$\frac{\delta f^+}{\delta t} = -e_{n+}f^+ + e_{n0}f^0, \quad (15)$$

$$\frac{\delta f^0}{\delta t} = -e_{n0}f^0. \quad (16)$$

According to the model, three emission reactions are possible: Two of these, $X^{(+|2+)}$ in Eq. (7) and the first process in Eq. (8), $X^{(0|+)}$, produce single exponential population decays, while the third process, $X^{((0)+|2+)}$ [the second step in Eq. (8)] is shown to induce a nonexponentiality into the capacitance transient [18]. Whenever necessary, we plot the peaks produced by these partial-emission processes in the figures. In deriving these equations, the recapture of emitted carriers in an electric field is neglected. As we see later in the O-DLTS experiments, however, the ON and OS defects are capable of capturing majority charges optically created in the space-charge region while these are being rapidly swept out by the electric field. The situation in the O-DLTS experiments is thus similar to the recapture of emitted carriers and indicates that this simplification introduces an error in the analysis. Because of difficulties in modeling the recapture process, the simplification is, however, unavoidable.

A complication in DLTS experiments further arises during the filling pulse, when the applied voltage is changed from reverse bias (-10 V here) to the filling-pulse voltage (0 V) and the extent of the space-charge region, in the depletion approximation, shrinks from a distance x_1 from the Schottky contact to a distance x_0 . As the built-in voltage (V_{bi}) of the metal-semiconductor contact prevents the space-charge region from being completely collapsed under these conditions, the capture rates of the deep levels are modified in the transition region of the space-charge region between the metal-semiconductor interface at $x = 0$ and x_0 due to a free-carrier tail with a density exponentially decaying from

the bulk density. The capture rate in the transition region is thus modified to [20]

$$c_{n(x)2+,n(x)+}(x) = c_{n2+,n+} \exp -0.5 \left(\frac{(x_0 - x)}{L_D} \right)^2, \quad (17)$$

while the capture rate in the region between x_0 and x_1 , containing a uniform free-carrier density, is given by Eq. (9). We refer to the literature for the calculation of the Debye length L_D and the points x_0 and x_1 in the space-charge region [20]. The total fractions of occupied levels entering Eq. (1) is then numerically integrated over the space-charge region, and this allows us to use measurements with filling-pulse lengths in the 50×10^{-9} – 50×10^{-6} s range in the multispectra fits despite the large capture cross sections. In contrast to electrical filling pulses, the optical pulses in OE-MCTS saturate all traps from the interface ($x = 0$) to the edge of the reverse-biased space-charge region (x_1). Since the minority-carrier diffusion lengths are several times larger than the extent of the space-charge region, we may assume an approximately uniform minority-carrier density and uniform trap filling after the long 100×10^{-3} s optical pulses.

As a test, the model is used to analyze DLTS measurements of the well-known $Z_{1/2}$ defect in 4H-SiC, which is made up of two negative- U defects with separate $Z_{1/2}^{(-|0)}$ but overlapping $Z_{1/2}^{(2-|0)}$ emission peaks [1]. The model is found to adequately describe the capture and emission behavior of both transitions of both defects [1].

A central aspect of the modeling process is the description of the capture cross-section temperature dependence, which we describe as either a multiphonon process or a two-stage cascade capture process. In the multiphonon process, capture and emission are accompanied by large lattice vibrations which give an exponential temperature dependence

$$\sigma(T) = \sigma_\infty \exp \frac{-E_\infty}{k_B T}, \quad (18)$$

where σ_∞ is generally in the range of 10^{-14} – 10^{-15} cm² and the barrier heights E_∞ may be tens to hundreds of meV, depending on which phonons are involved. Negative barrier heights are discussed by Henry and Lang to be possible for capture into a Coulomb-attractive level with barrier lowering due to a locally enhanced charge-carrier concentration [21].

In the two-stage cascade capture model for capture into deep Coulomb-attractive levels, the electron is initially captured into a shallow excited level of energy depth E_1 , followed by a transition to a deeper ground state by a thermally activated multiphonon process with energy barrier E_∞ [22]. The result is a temperature dependence of the form

$$\sigma(T) = AT^{-2} \exp \frac{-\Delta E}{k_B T}, \quad (19)$$

where A is a proportionality constant and the total energy barrier is defined as $\Delta E = E_\infty - E_1$. A negative ΔE may occur for a combination of a small multiphonon barrier and a deeper first excited state, giving a negative temperature dependence of the cross section due to the increasing thermal emission from the shallow excited state. The inverse case results in an exponentially increasing capture cross section with temperature.

To estimate the errors of the fitting parameters given in Tables I–IV, we compare values calculated using different starting conditions for the nonlinear least-squares fitting to all samples. The enthalpies ΔH are found to vary by less than $\pm 2\%$ from sample to sample and when using different measurement batches. Capture cross-section prefactors A or σ_∞ vary by less than $\pm 30\%$, while the capture-barrier ΔE error is less than $\pm 20\%$. The entropy factors χ are all found to be very small, and setting the entropy factor to 1 does not significantly degrade the quality of the fit. Values are given in Tables I–IV.

For the simulation of the TRPL carrier lifetimes, we use a model similar to the one described by Klein [23]. After the optical injection of excess electrons δ_n and holes δ_p added to the equilibrium electron n_0 and hole p_0 population, the band-to-band photoluminescence intensity is

$$I_{PL}(t) = \gamma[p_0 + \delta p(t)][n_0 + \delta n(t)] \quad (20)$$

with radiative recombination coefficient γ . Furthermore, a minority-carrier lifetime can also be calculated as

$$\tau_{min} = \left[-\frac{d\delta_{min}}{dt} \right]^{-1}, \quad (21)$$

where the minority carriers (min) are either holes or electrons in *n*- or *p*-type material, respectively. The decay of δ_n and δ_p by recombination via deep levels is numerically calculated by solving the coupled differential equations

$$\frac{d\delta_n}{dt} = - \sum_0^N R_{n,i}, \quad (22)$$

$$\frac{d\delta_p}{dt} = - \sum_0^N R_{p,i}, \quad (23)$$

where $R_{n,i}$ and $R_{p,i}$ are electron- and hole-capture rates, respectively, determined by the deep levels. In addition to these two differential equations, additional equations describing the population change of each deep level must be included. For details on the equations describing recombination via multilevel defects, we refer to the

literature [23]. The simulation is performed without the inclusion of carrier drift or diffusion and without surface recombination so as to focus only on the effect the oxidation-induced defects have on the carrier lifetime.

IV. RESULTS AND DISCUSSION

The DLTS spectra from as-grown 4*H*-SiC *n*-type epilayers in Fig. 1(a) are dominated by the V_C related defects $Z_{1/2}$ and $EH_{6/7}$. After their removal by oxidation-induced in-diffusion of C_i , three new distinct peaks, labeled ON1, ON2a, and ON2b, are found. The ON1 peak, as shown later, is the product of a completely overlapping two-electron emission process, and we plot the $ON1^{(0|+)}$ and $ON1^{((0|+)|2+)}$ partial transitions from the completely filled defect in the figure. The same defects are found by MCTS in *p*-type 4*H*-SiC oxidized at 1300 °C for 2 × 5 h. The spectrum in Fig. 1(b) shows the minority (electron) emission occurring at temperature positions almost identical to the *n*-type spectra. The ON1 peak is slightly shifted due to its overlapping emission structure, and the ON2b level occurs only as a shoulder next to the large ON2a peak.

In 6*H*-SiC, a similar situation presents itself, where the $E1/E2$ and R deep levels dominate the as-grown material spectra but are removed by the oxidation process, as shown in Fig. 2(a). The spectrum then consists of six new deep-level emission peaks. While the ON deep levels in 4*H*-SiC appear at the same positions for all samples, the peaks labeled OS1a and OS1b in 6*H*-SiC appear shifted by several degrees Kelvin in spectra of samples grown in different reactors. We assume that this slight shift is due to changes in the local defect environment, as different reactors may produce material with vastly different densities of intrinsic and extrinsic electrically active or inactive

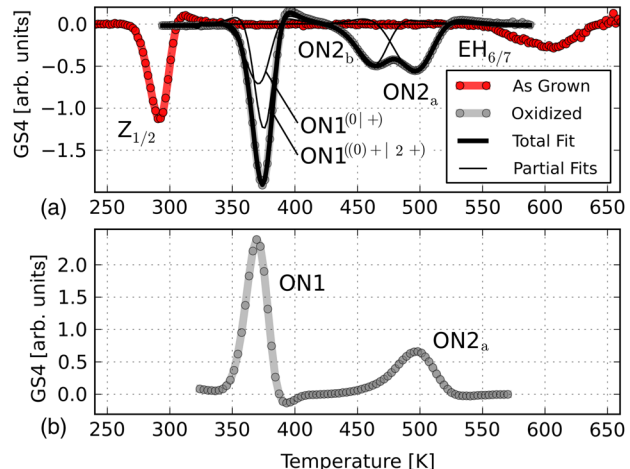


FIG. 1. (a) DLTS spectra of as-grown and oxidized *n*-type 4*H*-SiC. (b) MCTS spectrum of oxidized *p*-type material. The ON1 peak is shifted slightly due to its positive-*U* nature, and its amplitude is decreased by hole capture into the doubly-electron-occupied defect. ON2b is almost not visible due to hole capture.

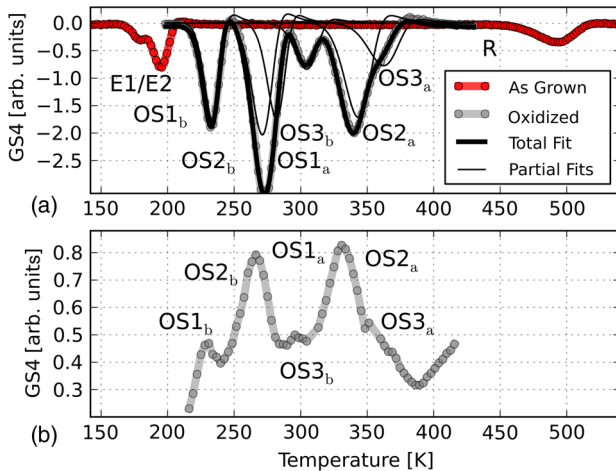


FIG. 2. (a) DLTS spectra of as-grown and oxidized *n*-type 6H-SiC. (b) MCTS spectrum of oxidized *p*-type material. OS1_b and OS3_b amplitudes are reduced by hole capture, while the amplitude reduction of OS2_b is partially obscured by peak overlap with OS1_a.

defects and slightly different strain states of the epilayer. As in 4H-SiC, the MCTS spectrum of *p*-type 6H-SiC oxidized at 1300°C for 2 × 5 h shown in Fig. 2(b) also shows minority (electron) emission at identical temperature positions. Compared to the 6H-SiC *n*-type spectra, the OS1_b and OS2_b peaks and the overlapping peak made up of OS1_a and OS2_b all appear with decreased amplitudes.

Our initial discussion focuses on the ON1 deep level in 4H-SiC, since the model which can be developed most clearly for this deep level also applies to the other levels. Next, ON2a and ON2b are discussed, followed finally by a discussion of the OS levels in 6H-SiC.

A. Oxidation-induced defects in 4H-SiC

The ON1 defect is modeled as being made up of either one or more single-level defects or a single two-level defect. Within the two-level model, different combinations of capture and emission processes are used: Both capture processes are simulated either as a multiphonon mechanism (MM), a combination of a two-stage cascade process followed by multiphonon capture of the second electron (CM), or two two-stage cascade processes (CC). In all cases, the barrier heights are allowed to vary freely from negative to positive, and the fits are tested with and without the inclusion of the entropy factor χ . All two-level models are found to give excellent fits to the sets of three to six spectra with filling pulses ranging from 50×10^{-9} to 50×10^{-6} s, and a plot of a three-spectra fit is given in Fig. 3(a). The single-level models, in contrast, are found to describe neither the sharp peak shape nor the filling-pulse behavior correctly [Fig. 3(b)], which agrees with our previous findings [24]. The sharpness and depth of the ON1 peak is a direct result of the nonexponential transient

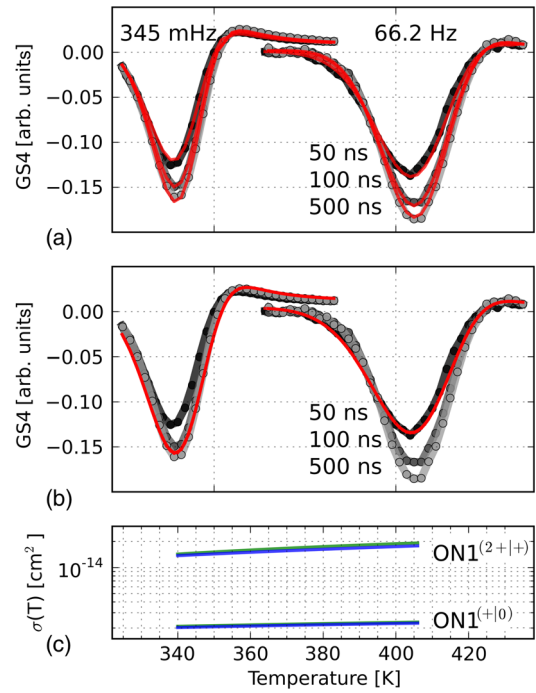


FIG. 3. (a) DLTS measurements of the ON1 defect in oxidized *n*-type 4H-SiC measured with three different filling-pulse lengths. The minimum (345 mHz) and maximum (66.2 Hz) emission-rate windows are shown. The multispectra fits using (a) a two-level (CM) and (b) a single-level model are displayed in red. Although the peak center position is fitted correctly, the single-level model cannot accurately describe the sharp peak shape and the filling-pulse behavior, leading to a best fit in which all three simulated curves completely overlap. (c) The temperature dependence of the electron-capture cross sections for the two different models (MM) and (CM), in blue and green, respectively, give nearly indistinguishable temperature dependencies almost completely identical with each other, leading to the blue curve almost completely overlapping the green curve.

distortion produced by the emission of the second electron (ON1^{((0)+|2+)}). In addition to the ON1 defect concentration being half of the DLTS measured concentration due to the two-electron emission process, the nonexponentiality then leads to further overestimation of the ON1 defect concentration when trying to calculate it based on a single-level assumption. The fit parameters for the two-level (CM) and (MM) models are given in Table I, and we find the measured capture cross sections to increase with the temperature, as shown in Fig. 3(c). Within the framework of the two-stage cascade capture process, this indicates an initial capture into a shallow excited state upon which the electron must overcome a large multiphonon barrier to relax to the ground state. It is evident, however, that even after tracking the peak over 70 K by measuring capacitance transients of 10-s length and more, a distinction between a purely exponential multiphonon capture process and a mixed power-law–exponential two-stage cascade capture process is impossible. The inclusion or exclusion of the

TABLE I. ON1 fitting parameters in *n*- and *p*-type material. In the fit of the hole-capture cross section, a multiphonon process is originally assumed. Parameters for the two-level models (CM) and (MM) are given. The resulting capture cross sections $\sigma(T)$ are given for the measurement temperature range of 340–410 K. E_b refers to the capture barrier, which is either E_∞ in the multiphonon case or $\Delta E = E_\infty - E_1$ in the two-stage cascade process. The given parameters are the best fits to the data; errors are discussed in Sec. III.

Transition	Mechanism	ΔH (eV)	χ	A (cm^2/K^2), σ_∞ (cm^2)	E_b (eV)	$\sigma(T)$ (cm^2)
ON1 ⁽²⁺⁺⁾	Two-stage cascade	0.88	~1–1.5	$A = 9.5 \times 10^{-8}$ $\sigma_{n,\infty} = 6.2 \times 10^{-14}$	0.11	$(1.8\text{--}2.6) \times 10^{-14}$
	Multiphonon	0.88	~1–1.5		0.044	$(1.4\text{--}2.0) \times 10^{-14}$
ON1 ^(+ 0)	Multiphonon	0.82	~1–2	$\sigma_{n,\infty} = 4 \times 10^{-15}$	0.02	$(2.0\text{--}2.3) \times 10^{-15}$
ON1 ^(0 +)	<i>T</i> -independent			$\sigma_{p,\infty} = 1.3 \times 10^{-17}$	0.00	1.3×10^{-17}

entropy term χ has only a minimal influence on the quality of the fit, and the term is around 2 for the second capture process, leading to a difference between ΔG and ΔH of less than 10 meV. This is in stark contrast to the well-known negative-*U* defect $Z_{1/2}$, where the capture of the second electron produces a significant structural relaxation of the defect and the entropy term for the second electron capture is very large. An optimal fit to the ON1 spectra is achieved assuming a positive-*U* configuration, where the second electron is bound less strongly than the first due to mutual repulsion. By switching the configuration to negative-*U*, a next-best fit with slightly worse sum-square errors is produced with different locations of the defect levels in the gap. A feature distinguishing the positive- and negative-*U* configurations is the direction of the peak shift as the filling-pulse length is reduced and the ratio of singly to doubly occupied levels changes. In the positive-*U* configuration the peak is expected to shift by approximately 4 K to lower temperatures, while in the negative-*U* configuration the peak is expected to shift to higher temperatures.

A confirmation of the positive-*U* two-level model is provided by the MCTS and OE-MCTS measurements on *p*-type samples in Fig. 4. An initial optical pulse of 300×10^{-3} s length is used to saturate the ON1 defects with the maximum number of electrons possible in a MCTS measurement. By applying an electrical pulse of varying length directly thereafter (OE-MCTS), we find that the peak amplitude is decreased by hole capture as a function of the pulse width until it has dropped to approximately 60% of its initial amplitude after a 1×10^{-4} s electrical pulse. At this point, hole capture ceases, even when increasing the electrical (hole) filling-pulse length to 1×10^{-2} s. The OE-MCTS results therefore are a clear indication that the ON1 defect is capable of hole capture when occupied by two electrons. Upon the emission of one electron, however, the defect becomes repulsive to holes, and a second hole cannot be captured. The slight peak shift to lower temperatures evident in Fig. 4 as the total defect population changes from a mixture of singly and doubly occupied ON1 defects to purely singly-electron-occupied defects is more clearly visible in Fig. 5. Here, we apply the multispectra fitting method to extract σ_{p0} of the

doubly-electron-occupied level. As we cannot determine the exact initial occupation ratio of ON1 due to uncertainty of the electron and hole density in the space-charge region, we allow the initial ratio of doubly to singly occupied levels to vary as a polynomial over the temperature. This initial occupancy ratio applies to all five spectra in the multispectra fit, and σ_{p0} is then derived from the relative changes in peak heights determined by the width of the electrical filling pulse according to Eq. (6). The resulting fit to all spectra gives a temperature-independent σ_{p0} for the doubly-electron-occupied level approximately 2–3 orders of magnitude smaller than σ_{n2+} and σ_{n+} [see Table I and Fig. 3(c)], and the ON1 defect is found to follow the approximately 4-K peak position shift expected from the positive-*U* model derived from the DLTS data. ON1 is thus found to be only a very inefficient recombination center. A similar peak shift is found in the O-DLTS spectra in Fig. 6, where the ON1 defect efficiently captures single

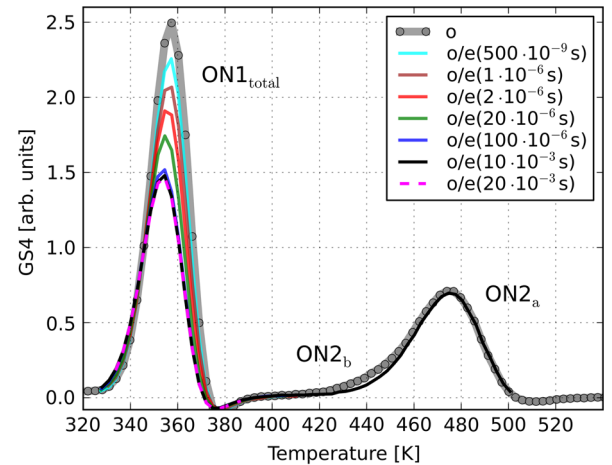


FIG. 4. MCTS and OE-MCTS measurements on *p*-type 4H-SiC using a 100×10^{-3} s optical pulse to saturate the defects with electrons, followed by an electrical majority (hole) filling pulse of increasing length. ON2b is almost empty due to hole capture competing with the electron capture, while the ON2a peak amplitude is not influenced by the electrical majority filling pulses, indicating that the level does not capture holes. The ON1 peak amplitude decreases until all defects are singly electron occupied, upon which hole capture ceases.

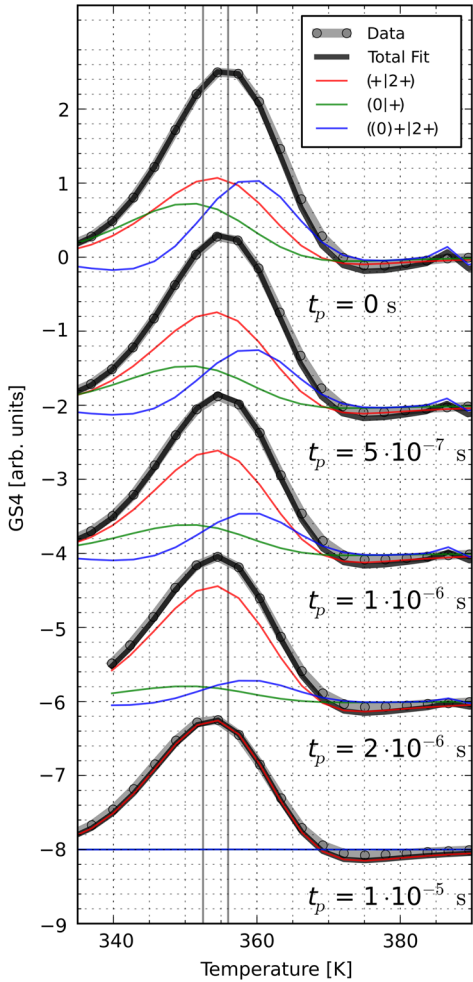


FIG. 5. MCTS and OE-MCTS on ON1 in *p*-type 4H-SiC from Fig. 4 with two-level (CM) model fits and peaks shifted for better visibility. As the electrical hole filling-pulse length increases, the number of levels occupied by two electrons decreases, reducing the ON1^(0|+) (green) and ON1^{((0)+|2+)} (blue) emission components. For long filling pulses, only singly-electron-occupied levels remain, and ON1^(+|0) (red) dominates. The experimentally found approximately 4-K peak shift to lower temperatures (indicated by the vertical lines) is reproduced by the model.

majority carriers (electrons) optically created in the space-charge region with densities varying from 3×10^{11} to $7 \times 10^{14} \text{ cm}^{-3}$ by pulses of up to $30 \times 10^{-3} \text{ s}$ length, despite these being rapidly swept out by the electric field. The capture of the second electron competes with the capture of the significantly higher density of holes, and the full peak amplitude expected from DLTS measurements is never reached. We also find the EH_{6/7} deep level in as-grown material to be able to capture majority electrons in *n*-type O-DLTS measurements, where specifically the EH₇ is assigned to the donor level ^(+|0) of the V_C [25]. In analogy again to the doubly occupied ON1⁽⁰⁾, the EH_{6/7} deep level in *p*-type material is also found to have only a very small hole-capture cross section when occupied by

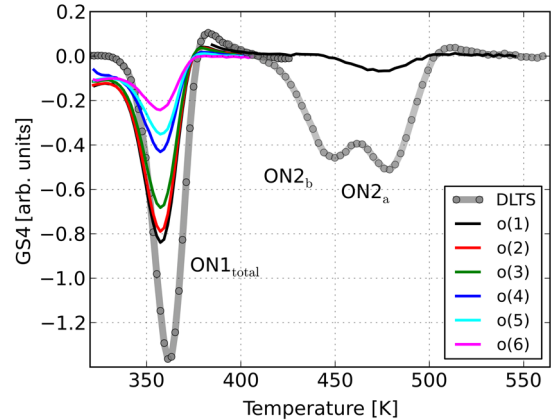


FIG. 6. DLTS ($100 \times 10^{-9} \text{ s}$ electrical filling pulse) and OE-DLTS measurement using only optical filling pulses of increasing power on oxidized *n*-type 4H-SiC. Electron capture into the attractive ON1 level occurs rapidly, and the peak shift produced by the single-electron occupation is visible. ON2a appears far less attractive to electrons in the electric field, while ON2b is empty due to competing hole capture.

one electron [26]. Based on these similarities, we propose ON1 to have double-donor character, with emissions from the doubly and singly occupied levels overlapping almost completely. The defect appears Coulomb attractive to electrons due to having excited states near the conduction band which enable the capture of the electrons in the presence of an electric field in the O-DLTS experiments. Once completely occupied and neutral, the capture of a single hole may occur with a small capture rate.

D-DLTS and R-DLTS measurements do not show any field-dependent barrier lowering for a capture into the ON1 defect. However, a lack of field dependence does not give any clear indication of charge state, since it is shown that the existence of a capture barrier may distort a Coulomb-attractive long-range potential enough to make the barrier-lowering effect negligible [27]. This is again similar to the case of EH_{6/7}, which is also found to exhibit no pronounced electric-field dependence [28].

In summary, the ON1 deep-level peak in DLTS could successfully be fitted over a temperature range of 70 K as emission from a positive-*U* two-level defect, where specifically the ON1^{((0)+|2+)} emission process is found to create a nonexponentiality of the decay. The doubly occupied ON1⁽⁰⁾ deep level is found to capture holes with a very small capture cross section, while the single-electron-occupied ON1⁽⁺⁾ is repulsive to holes. From comparison with the capture behavior of EH_{6/7}, we suggest the defect to have double-donor character.

Switching to the ON2a and ON2b levels, our analysis follows the same procedure outlined for the ON1 defect above. We compare single- and two-level models with different combinations of capture mechanisms [(MM), (CM), and (CC)] and find the two-level models to give almost indistinguishably good results when fitting six

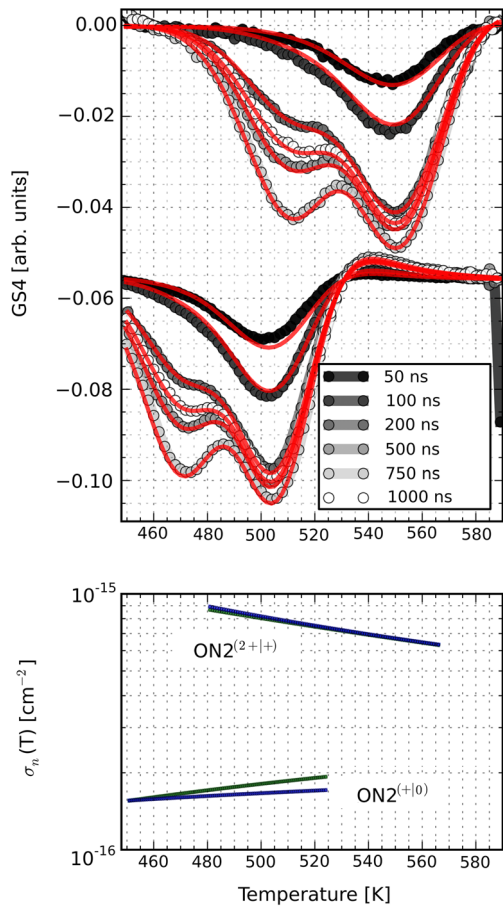


FIG. 7. (a) Fitting of ON2a and ON2b using the two-level (CM) model. Both 80.7 (top) and 11.3 Hz (bottom) emission-rate windows are spectra calculated from the same measured data. (b) The temperature dependence of σ_{n2+} and σ_{n+} derived using either the (MM) and (CM) two-level models is only minimally different.

spectra simultaneously, as shown in Fig. 7. The fit parameters are given in Table II. The entropy factors χ are again found to have minimal influence on the fit quality and produce a difference between ΔG and ΔH of less than 50 meV, enforcing the positive- U behavior of the defect. As the peaks are well separated and show no clearly visible nonexponentiality, one may assume they are uncoupled

TABLE II. ON2 fitting parameters in *n*- and *p*-type material, with resulting capture cross sections $\sigma(T)$ given for the experiment's temperature range of 440–530 K. For the hole-capture cross section, we originally assume a multiphonon process, and the value is only a rough estimate. E_b refers to the capture barrier, which is either E_∞ in the multiphonon case or $\Delta E = E_\infty - E_1$ in the two-stage cascade process. The given parameters are the best fits to the data; errors are discussed in Sec. III.

Transition	Mechanism	ΔH (eV)	χ	A (cm ² /K ²), σ_∞ (cm ²)	E_b (eV)	$\sigma(T)$ (cm ²)
ON2 ⁽²⁺⁺⁾	Two-stage cascade	1.06	$\sim 1\text{--}2$	$A = 2.0 \times 10^{-10}$	-0.005	$(10\text{--}6) \times 10^{-16}$
	Multiphonon			$\sigma_{n,\infty} = 1.1 \times 10^{-16}$	-0.092	$(10\text{--}7) \times 10^{-16}$
ON2 ⁽⁺⁾⁰	Two-stage cascade	0.98	$\sim 1\text{--}2$	$A = 1.4 \times 10^{-10}$	0.061	$(2.4\text{--}2.0) \times 10^{-16}$
	Multiphonon			$\sigma_{n,\infty} = 6.5 \times 10^{-16}$	0.04	$(2.8\text{--}3.3) \times 10^{-16}$
ON2 ⁽⁰⁺⁾	<i>T</i> -independent			$\sigma_{p,\infty} = 1.0 \times 10^{-16}$	0.00	$\leq 1 \times 10^{-16}$

single levels. We test this hypothesis in Fig. 8 and find that the fit with single-level models produces larger sum-square errors but not as severe as in the case of ON1. It is also unable to provide a physical reason for the constant concentration ratio between the levels, nor does it provide any explanation for the hole-capture behavior found in the MCTS and OE-MCTS experiments.

Apart from the greater difference in emission rate between the levels, we find that all capture mechanisms possess negative barrier heights for σ_{n2+} , producing a negative temperature dependence, as seen in Fig. 7. Within the context of the two-stage cascade model, this indicates that the electron has a very small multiphonon barrier to overcome after capture into a shallow excited state, increasing the chance for reemission as the temperature is increased. Similar to ON1, the capture cross section σ_{n+} is smaller than σ_{n2+} and shows a positive temperature dependence.

The MCTS and OE-MCTS spectra in Figs. 1 and 4 and DLTS and O-DLTS spectra in Fig. 6 give clearer evidence that the two-level model applicable to ON1 also applies to ON2a and ON2b. In Fig. 4, we find that, although ON2a can be saturated with electrons and does not decrease in amplitude even after 1×10^{-2} s electrical (hole) injection pulses, the ON2b peak appears only as a shallow shoulder to ON2a and completely disappears after the electrical pulse. In the O-DLTS spectra, seen in Fig. 6, ON2b is not visible, but even ON2a cannot be filled to a significant level. Since we know from OE-MCTS that this cannot be due to hole capture, the origin for this behavior may be the small electron-capture cross section. Only a rough estimate of σ_{p0} is possible based on the spectra, as the vanishing peak amplitude precludes any accurate filling-pulse measurements, and we find it to be equal to or smaller than 1×10^{-16} cm² for ON2⁽⁰⁾. For the later TRPL carrier-lifetime simulation, we vary it from 1×10^{-17} to 1×10^{-16} cm². Measuring the field dependence of the emission by R-DLTS shows a small peak-amplitude change as a function of the electric field, which, however, is not enough for an accurate quantification. Based on the DLTS, O-DLTS, MCTS, and OE-MCTS spectra and their similarities to ON1, we conclude that the ON2a and ON2b

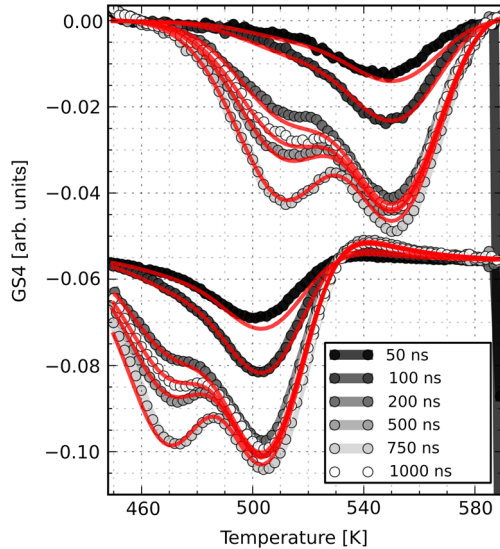


FIG. 8. Alternative fitting of ON2a and ON2b using two single-level models. Both 80.7 (top) and 11.3 Hz (bottom) emission-rate windows are spectra calculated from the same measured data. The quality of the fit is inferior to that of the two-level model, and a model using two independent single levels further offers no explanation for the OE-MCTS results in Fig. 4 and the fixed concentration relation between ON2a and ON2b.

peaks also originate from a positive- U two-level defect. ON2a is composed of the overlapping emission processes $\text{ON2}^{(+|2+)}$ and $\text{ON2}^{((0)+|2+)}$, while ON2b is the first electron emission of a doubly occupied level, $\text{ON2}^{(0|+)}$.

Using the coupled-level models to account for the two electron emissions from each defect and the unique peak shape of the ON1 defect, we are now able to correctly calculate the ON1 and ON2 densities in oxidized 4H-SiC. The deep-level concentrations are measured within the top 1.5–4 μm of the epilayer (based on sample doping and the 0-V DLTS pulse bias and –10-V reverse bias used), and their dependence on the oxidation temperature and duration is given in Table III. Their profiles, measured by D-DLTS, appear quite flat in the measured volume and decrease only slightly when moving away from the surface. Surprisingly, the *p*-type sample shows ON1 and ON2 concentrations slightly

TABLE III. Densities of ON1 and ON2 deep levels measured in the top 4 μm of the epilayers for three samples oxidized at three different temperatures. The deep-level density ratio is found to be approximately 1:1.

Temperature (°C)	Duration (min)	Doping	ON1 (cm^{-3})	ON2 (cm^{-3})
1300	900	Nitrogen (<i>n</i>)	5.7×10^{12}	5.7×10^{12}
1300	2x 300	Aluminum (<i>p</i>)	5×10^{13}	5×10^{13}
1400	1000	Nitrogen (<i>n</i>)	1.0×10^{13}	1.0×10^{13}
1500	1000	Nitrogen (<i>n</i>)	4.4×10^{13}	4.4×10^{13}

higher than in similar *n*-type samples. All samples, *n*- and *p*-type, consistently show a very similar ON1:ON2 concentration ratio of 1:1, and the deep-level concentrations are independent of the doping concentrations in the measured samples.

B. Oxidation-induced defects in 6H-SiC

The situation in 6H-SiC is more complex due to the number of peaks (six) and the extreme overlap of OS2a with OS3a and OS1a with OS2b (see Figs. 2 and 9). The latter two can be resolved when using rate windows

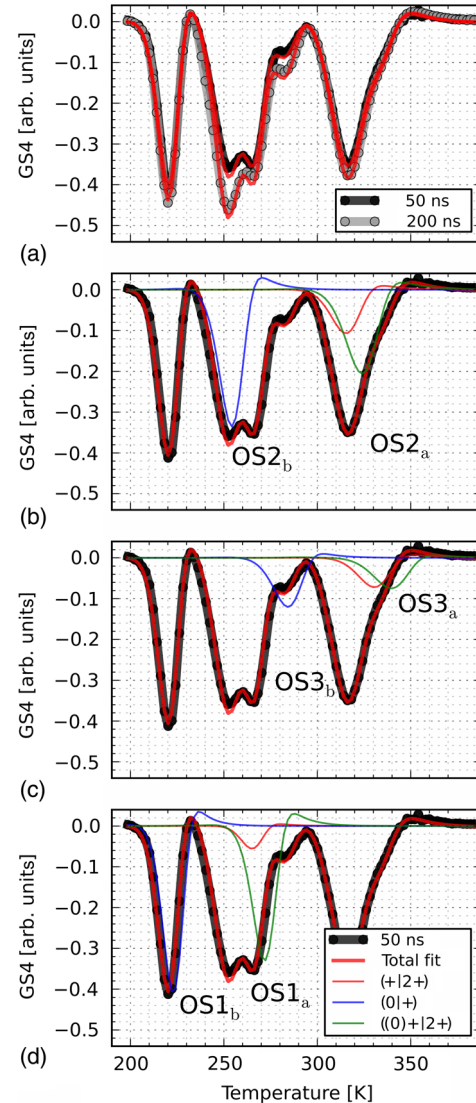


FIG. 9. (a) DLTS spectra of an oxidized *n*-type 6H-SiC sample with filling-pulse lengths of 50×10^{-9} and 200×10^{-9} s. The multispectra fit using three two-level (CM) models fits the measured spectra well. In (b)–(d), the measurement with a 50×10^{-9} s filling pulse is separated into the partial emission processes. OS2b–OS3b result from the $(0|+)$ transition processes, while OS1b–OS3a result from the $(+|2+)$ and $((0)+|2+)$ transitions of the OS1–OS3 defects.

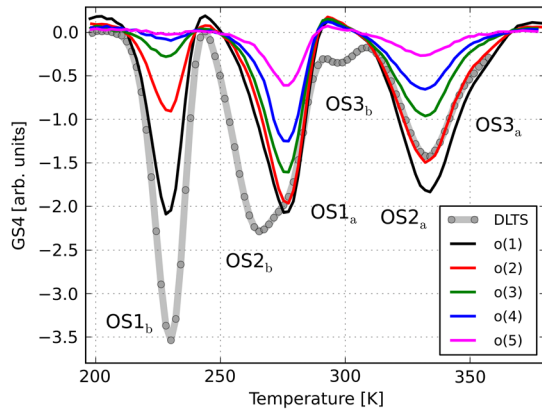


FIG. 10. DLTS (100×10^{-9} s electrical filling pulse) and O-DLTS measurement using only optical filling pulses of increasing power [from o(5) to o(1)] on oxidized *n*-type 6*H*-SiC. The OS1a, OS2a, and OS3a levels rapidly capture electrons, while OS2b and OS3b remain nearly empty due to hole capture. The OS1a amplitude appears to decrease only once OS1b is nearly empty.

derived from transients several seconds long. Before applying the six single-level or three two-level models with (MM), (CM), and (CC) capture cross-section combinations, a qualitative review of the DLTS data in Fig. 9 and the O-DLTS data in Fig. 10 is required to determine which levels may be coupled: The peak amplitude ratios indicate that the levels fall into two groups, with group one made up of OS1a, OS1b, OS2a, and OS2b and group two made up of OS3a and OS3b. The grouping suggests a relation to the three inequivalent lattice sites of 6*H*-SiC, with group-one levels related to the cubic sites (k_1 , k_2) and group-two levels related to the single hexagonal (h) lattice site.

From O-DLTS in Fig. 10, we find that the levels OS1b and OS2b may only be partially filled with optically excited majority electrons due to competing hole- and electron-capture processes and the rapid removal of electrons from the space-charge region by the electric field. OS3b is not filled at all, while levels OS1a, OS2a, and OS3a can be completely saturated and appear to be

repulsive to the concurrently injected large concentration of holes. The same difference in electron occupation is also found in the MCTS spectra in Fig. 2 measured on the oxidized *p*-type sample, showing the OS1b, OS2b, and OS3b levels to be capable of capturing holes while the OS1a, OS2a, and OS3a levels appear hole repulsive. All levels are further found to be stationary in their temperature positions when using different optical pulse lengths in O-DLTS and OE-MCTS, and we can exclude ON1-like overlap of the two electron-emission processes. The MCTS and OE-MCTS spectra are, however, of too low quality to accurately estimate any hole-capture cross sections. Finally, the small difference in the positions of the OS1a and OS1b peaks between materials grown in different reactors and their greater ability to capture electrons as compared to OS2a and OS2b in Fig. 10 leads us to the conclusion that level coupling exists between OS1a and OS1b, OS2a and OS2b, and OS3a and OS3b. The multispectra fit using three positive-*U* two-level (CM) models for the defects fitted to spectra with filling pulses from 140×10^{-9} to 500×10^{-9} s is shown in Fig. 9, and the resulting fit parameters are given in Table IV. Similar again to the ON defects in 4*H*-SiC, the entropy factor is found to be close to one, so that ΔG and ΔH again differ by less than 10 meV. We find the absolute defect concentrations to be larger by roughly an order of magnitude when compared to 4*H*-SiC, and the OS1:OS2:OS3 ratio is found to be 3:3:1, irrespective of oxidation conditions. We also test fitting of the spectra using a set of six single-level models with a different capture mechanism. The fits to individual spectra are excellent; however, the effective capture cross sections derived this way scatter over almost 3 orders of magnitude. Attempts to perform multispectra fits are not successful, and no viable model of the deep levels and their capture behavior can be produced by single-level models.

C. The influence on carrier lifetime

Using the complete model of the electron- and hole-capture processes at the ON defects, the influence on the charge-carrier lifetime in *n*- and *p*-type material can now be

TABLE IV. Fitting parameters for the DLTS spectra measured on oxidized *n*-type 6*H*-SiC, with resulting capture cross sections $\sigma(T)$ given for the measurement temperature range of approximately 50 K around the deep levels in Fig. 10. E_b refers to the capture barrier, which is either E_∞ in the multiphonon case or $\Delta E = E_\infty - E_1$ in the two-stage cascade process. The given parameters are the best fits to the data; errors are discussed in Sec. III.

Transition	Mechanism	ΔH (eV)	χ	A (cm^2/K^2), σ_∞ (cm^2)	E_b (eV)	$\sigma(T)$ (cm^2)
OS1 ^(2+ +)	Two-stage cascade	0.80	~ 1	$A = 1.2 \times 10^{-9}$	0.025	$(6.3\text{--}5.5) \times 10^{-16}$
OS1 ^(+ 0)	Multiphonon	0.63	~ 1	$\sigma_{n,\infty} = 6.5 \times 10^{-16}$	0.005	3.2×10^{-16}
OS2 ^(2+ +)	Two-stage cascade	0.82	~ 1	$A = 9.0 \times 10^{-11}$	-0.038	$(6\text{--}3.3) \times 10^{-16}$
OS2 ^(+ 0)	Multiphonon	0.69	~ 1	$\sigma_{n,\infty} = 1.0 \times 10^{-15}$	0.029	$(2.5\text{--}3.2) \times 10^{-16}$
OS3 ^(2+ +)	Two-stage cascade	0.65	~ 1	$A = 4.8 \times 10^{-8}$	0.078	$(8.8\text{--}14) \times 10^{-16}$
OS3 ^(+ 0)	Multiphonon	0.54	~ 1	$\sigma_{n,\infty} = 1.6 \times 10^{-14}$	0.028	$(9\text{--}12) \times 10^{-16}$

quantified. For this purpose, we simulate the minority-carrier lifetime using Eqs. (20)–(23) in the bulk of an *n*- or *p*-type sample of $1 \times 10^{15} \text{ cm}^{-3}$ doping density as a function of the concentration of ON1 and ON2. The only parameter which cannot be determined with any precision, σ_{p0} of the ON2 defect, is varied from 1×10^{-17} to $1 \times 10^{-16} \text{ cm}^2$. Since the charge-carrier lifetime is injection-level dependent and since the ON1 and ON2 defect concentrations reach up to mid $\times 10^{13} \text{ cm}^{-3}$ levels, we define a lifetime $\tau_{\min(\delta_{\min}=N_{\text{dop}})}$ using Eq. (21) for the following analysis. The instantaneous minority-carrier lifetime at this point, where the excess minority-carrier density equals the doping density, provides a point which is accessible by TRPL measurements, can be easily compared between all simulations, and is far above the ON1 and ON2 defect densities. A realistic estimate of the remaining V_C defect concentration after oxidation is also required. For this purpose, a low-doped ($4 \times 10^{13} \text{ cm}^{-3}$) *n*-type sample is oxidized at 1300°C for 2 h. The initial V_C concentration before oxidation is $5 \times 10^{11} \text{ cm}^{-3}$, based on the $1 \times 10^{12} \text{ cm}^{-3}$ concentration of $Z_{1/2}$ measured by DLTS, which is an average concentration found in high-quality epilayers with *n*-type doping densities between 4×10^{13} and $8 \times 10^{15} \text{ cm}^{-3}$ [29]. The $Z_{1/2}$ center is completely removed from the spectra by the oxidation, and the concentration of V_C defects after the oxidation is below $1 \times 10^{10} \text{ cm}^{-3}$, based on the detection limit in this specific sample. From Eqs. (20)–(23) and the model for $Z_{1/2}$ given by Klein, a $1 \times 10^{10} \text{ cm}^{-3}$ concentration of V_C is expected to lead to a bulk $\tau_{\min(\delta_{\min}=N_{\text{dop}})}$ of approximately $320 \mu\text{s}$, while a concentration of $2 \times 10^{10} \text{ cm}^{-3}$ leads to approximately $260 \mu\text{s}$ [2]. This value is significantly larger than the lifetimes encountered in very thick epilayers ($>140 \mu\text{m}$) oxidized for very long durations or subjected to carbon implantation and annealing, where the longest reported carrier lifetime value is $33.2 \mu\text{s}$ [30,31]. The actual TRPL measured lifetime in the low-doped sample is $1.3 \mu\text{s}$ before and $3.5 \mu\text{s}$ after the oxidation. The sample thickness of only $44 \mu\text{m}$, however, represents a significant limiting factor. Since the $Z_{1/2}$ model contains a large number of adjustable parameters and since the exact identity of the lifetime-limiting defect(s) in *p*-type 4*H*-SiC is unclear, we replace $Z_{1/2}$ in the following analysis by a single-level midgap recombination center, referred to as R , which limits the bulk $\tau_{\min(\delta_{\min}=N_{\text{dop}})}$ to $300 \mu\text{s}$ in *n*- or *p*-type material.

In Fig. 11, we show TRPL decay curves (a), the instantaneous minority-carrier densities δn (b), and the instantaneous minority-carrier lifetimes τ_p (c) simulated for *n*-type material based on the above parameters, with and without ON1 and ON2 in concentrations of $2 \times 10^{13} \text{ cm}^{-3}$. The same for the case of *p*-type material is given in Fig. 12. An initial injection level of excess minority (δ_{\min}) and majority carriers (δ_{maj}) of $1 \times 10^{17} \text{ cm}^{-3}$ at the beginning

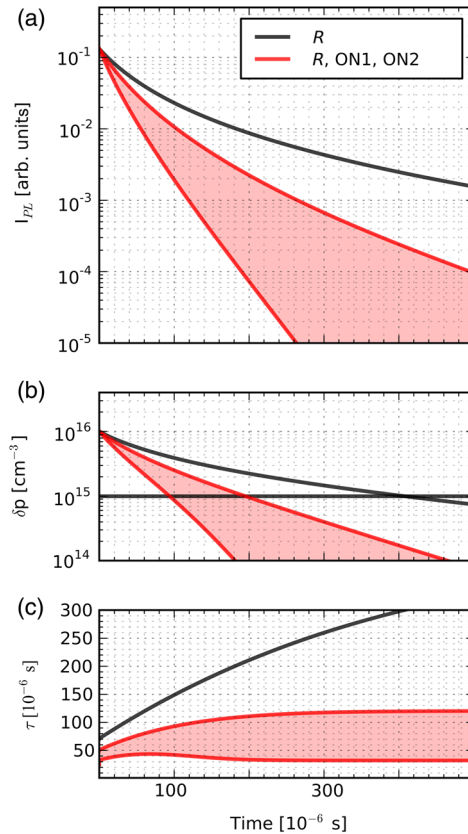


FIG. 11. TRPL decay curves (a), minority-carrier densities (b), and the instantaneous lifetime (c) simulated for *n*-type material with (red) and without (black) ON1 and ON2. The error spread (red) is due to the large error in determining $\sigma_{p0}(T)$ of ON2. In the absence of ON1 and ON2, the material is limited to a $\tau_{\min(\delta_{\min}=N_{\text{dop}})}$ of $300 \mu\text{s}$ (at approximately $350 \mu\text{s}$ on the time axis) by a stand-in recombination center R . The oxidation-induced defect density is $\text{ON1} = \text{ON2} = 2 \times 10^{13} \text{ cm}^{-3}$, and the horizontal line in (b) gives the doping density.

of the simulation ($t = 0 \text{ s}$) is used to explore the entire region from high- to low-injection conditions, and the simulation is performed at 300 K . While the TRPL intensity decay shape of oxidized material is expected to show a slight upward slant throughout the entire injection region in *n*-type material, the decay curve simulated in *p*-type material displays an obvious downward slant once δ_{\min} approaches the doping density. The difference is due to the hole- and electron-capture cross-section ratio of ON1 and ON2 and reproduces an effect which has been previously described in decay curves of oxidized samples in the literature [32]. Although it is ascribed there to the difference in ambipolar diffusion constants between oxidized *n*- and *p*-type material, the effect appears to also originate from the oxidation-induced defects. Despite this difference, for both conductivity types, the inclusion of ON1 and ON2 into the simulation increases the rate of charge-carrier recombination and lowers $\tau_{\min(\delta_{\min}=N_{\text{dop}})}$, as

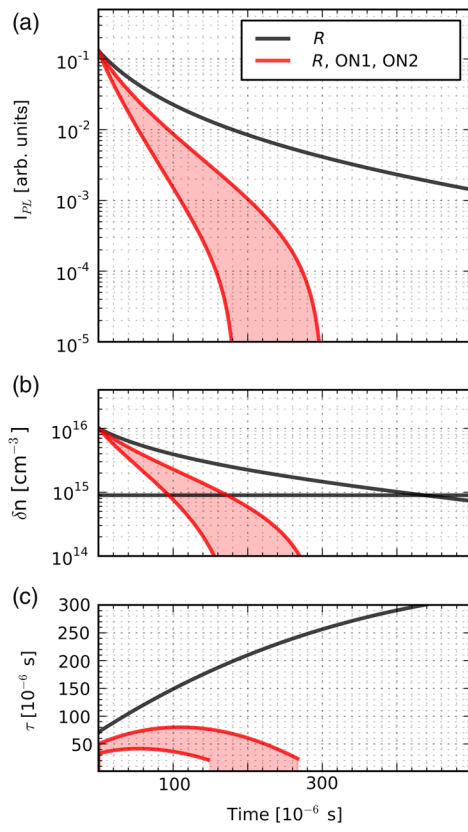


FIG. 12. TRPL decay curves (a), minority-carrier densities (b), and the instantaneous lifetime (c) simulated for p -type material with (red) and without (black) ON1 and ON2. The error spread (red) is due to the large error in determining $\sigma_{p0}(T)$ of ON2. In the absence of ON1 and ON2, the material is limited to a $\tau_{\min(\delta_{\min}=N_{\text{dop}})}$ of 300 μs (at approximately 350 μs on the time axis) by a stand-in recombination center R . The oxidation-induced defect density is $\text{ON1} = \text{ON2} = 2 \times 10^{13} \text{ cm}^{-3}$, and the horizontal line in (b) gives the doping density.

can be seen in Figs. 11(c) and 12(c). The effect on the mid- to low-injection range lifetime is stronger in p -type than in n -type material, which again concurs with the literature, where lifetime enhancement oxidations are found to be less effective in p -type material than in n -type material [33]. Other effects, such as a lower rate of diffusion for C_i in p -type relative to in n -type material, also further decrease the effectiveness of lifetime enhancement oxidations in p -type material.

This influence on $\tau_{\min(\delta_{\min}=N_{\text{dop}})}$ is further explored in Fig. 13, where we plot $\tau_{\min(\delta_{\min}=N_{\text{dop}})}$ as a function of the concentrations of ON1 and ON2, which are scanned from 1×10^{10} to $5 \times 10^{13} \text{ cm}^{-3}$ in n - and p -type epilayers limited to a lifetime of 300 μs in the absence of ON1 and ON2. The defects have a clear effect on the simulated bulk carrier lifetime once their concentration increases above $1 \times 10^{12} \text{ cm}^{-3}$ and appear to impose a limit on the maximum attainable bulk carrier lifetime in epilayers which have been subjected to lifetime enhancement

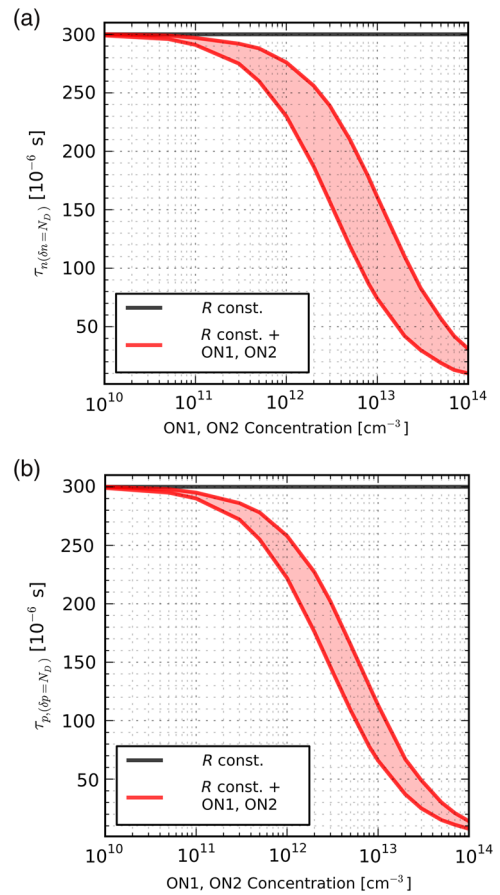


FIG. 13. The TRPL decay constant $\tau_{\min(\delta_{\min}=N_{\text{dop}})}$ as a function of ON1 and ON2 density in n -type (a) and p -type (b) material otherwise limited to a $\tau_{\min(\delta_{\min}=N_{\text{dop}})}$ of 300 μs in the absence of ON1 and ON2. The effect of ON1 and ON2 is slightly stronger in p -type material.

oxidations or carbon implantations and annealings. In the end, however, the efficiency of ON1 and ON2 as recombination centers in actual epilayers is far lower than that of $Z_{1/2}$, and the improvements gained in carrier lifetime by the lifetime enhancement processes ($\times 5$ or more) are significant.

Practically measuring the exact influence of ON1 and ON2 on the carrier lifetime by TRPL or microwave photoconductivity decay is currently made impossible by a number of factors. These are a strong influence of surface recombination due to a lack of good surface passivation schemes, difficulties in measuring the very low V_C concentration in oxidized material, the existence of an oxidation-process-related density profile in the ON1 and ON2 concentrations, and the lack of epilayers with combined very low ON1, ON2, and V_C concentrations for comparison.

No direct conclusions can be drawn on the capability of the OS defects to influence the carrier lifetime in 6H-SiC, since the hole-capture cross sections cannot be measured. Experimentally, we find the oxidations at 1300 °C to

increase the measured carrier lifetimes from approximately 80×10^{-9} s in the as-grown *n*-type and *p*-type material by a factor of 5–8 (to 400×10^{-9} – 700×10^{-9} s) and 2–3 (to 200×10^{-9} – 250×10^{-9} s), respectively. Based on the similarity between the oxidation-induced defects in 4*H*- and 6*H*-SiC, we expect that the OS defects have a similar influence on the bulk carrier lifetime in 6*H*-SiC epilayers.

D. Possible physical origin of the ON and OS defects

The formation of ON and OS defects by oxidation strongly points to the involvement of carbon interstitials C_i , which is further supported by the similarity of their measured concentration profiles to simulated C_i indiffusion profiles [11]. A direct involvement of oxygen appears unlikely, as the ON defects are also found in samples implanted with C^+ or Si^+ and annealed at a high temperature [11]. A proposed involvement of nitrogen from the gas phase seems unlikely, as our oxidations are performed in high-purity SiC crucibles in a flow of pure Ar mixed with pure dry O_2 [11]. The involvement of N dopants which are incorporated during epigrowth can also be excluded, since this would require a near-complete conversion of residual N in the *p*-type samples to create the measured approximately $1 \times 10^{14} \text{ cm}^{-3}$ total density. An involvement of boron can be excluded for the same reasons. The most likely candidates are defect complexes based on C_i in possible combination with other intrinsic defects, of which a large number of configurations are determined to be electrically active and thermally highly stable [34,35]. The occurrence of two ON defects in 4*H*-SiC at a concentration ratio of 1:1 and of three OS defects in 6*H*-SiC at a ratio of 3:3:1, apparently independent of sample growth and oxidation conditions, strongly links the defects to the inequivalent lattice sites of the polytypes. As intrinsic defects may, however, be constructed from a combination of elementary defects on inequivalent lattice sites ($C_{Si}-V_C$ can, for example, be formed on *hh*, *hk*, *kh*, and *kk* sites in 4*H*-SiC), we cannot exclude that each ON- and OS-defect peak set actually originates from more than one defect with very similar properties.

V. CONCLUSION

We measure the electrical properties of the deep levels ON1, ON2a, and ON2b in 4*H*-SiC as well as their 6*H*-SiC counterparts OS1a, OS1b, OS2a, OS2b, OS3a, and OS3b in both *n*- and *p*-type material. The uniquely narrow peak shape of ON1 and the peak center position shift as a function of the level occupation in DLTS and MCTS is determined to originate from an overlapping positive-*U*, two-electron emission process. Similar to $EH_{6/7}$, which is clearly identified as the $(2+|+)$ and $(+|0)$ donor levels of V_C , the ON1 defect is capable of capturing majority electrons supplied optically into the space-charge region

in *n*-type material, indicating a capture into a Coulomb-attractive defect with excited states near the conduction band which is then also repulsive to holes [25,26]. Hole capture is found to occur only into the doubly-electron-occupied (neutral) defect with σ_{p0} 2–3 orders of magnitude smaller than σ_{n2+} and σ_{n+} . Based on these data, we assign double-donor character to the ON1 deep level. Although all other levels (ON2a and ON2b and the OS defects in 6*H*-SiC) can be fitted as single-level defects in the individual DLTS, O-DLTS, MCTS, and OE-MCTS spectra, the fitting gives worse results or fails when simulating several spectra simultaneously with the same parameters. Multispectra fitting indicates them to also be positive-*U* coupled, most likely double-donor-type deep levels similar to ON1. The occurrence of a total of two oxidation-induced defects in 4*H*-SiC and three defects in 6*H*-SiC strongly points to C_i -based defects involving inequivalent lattice sites. Finally, from simulated TRPL decay curves and recombination rates at the deep levels, we conclude that the oxidation-induced defects are only very weak recombination centers which have a larger impact on the charge-carrier lifetime in *p*-type material than in *n*-type material. Although they are significantly less efficient recombination centers compared to $Z_{1/2}$, their large density as a by-product of the lifetime enhancement process and their thermal stability allow them to set a high upper limit on the bulk charge-carrier lifetime achievable by lifetime enhancement oxidations or carbon implantations or annealing. Since their density is highest in the first several micrometers of semiconductor material adjacent to the surface used for lifetime enhancement oxidation, this surface should be chosen carefully, so as to avoid large defect densities in current-carrying regions of devices [11].

ACKNOWLEDGMENTS

We gratefully acknowledge the financial support from the Swedish Foundation for Strategic Research (SSF) and the Swedish Research Council (VR).

-
- [1] C. G. Hemmingsson, N. T. Son, A. Ellison, J. Zhang, and E. Janzén, Negative-*U* centers in 4*H* silicon carbide, *Phys. Rev. B* **58**, R10119 (1998).
 - [2] P. B. Klein, B. V. Shanabrook, S. W. Huh, A. Y. Polyakov, M. Skowronski, J. J. Sumakeris, and M. J. O'Loughlin, Lifetime-limiting defects in *n*- 4*H*-SiC epilayers, *Appl. Phys. Lett.* **88**, 052110 (2006).
 - [3] C. G. Hemmingsson, N. T. Son, and E. Janzén, Observation of negative-*U* centers in 6*H* silicon carbide, *Appl. Phys. Lett.* **74**, 839 (1999).
 - [4] S. Sasaki, K. Kawahara, G. Feng, G. Alfieri, and T. Kimoto, Major deep levels with the same microstructures observed in *n*-type 4*H*-SiC and 6*H*-SiC, *J. Appl. Phys.* **109**, 013705 (2011).

- [5] A. Koizumi, V. P. Markevich, N. Iwamoto, S. Sasaki, T. Ohshima, K. Kojima, T. Kimoto, K. Uchida, S. Nozaki, B. Hamilton, and A. R. Peaker, E1/E2 traps in 6H-SiC studied with Laplace deep level transient spectroscopy, *Appl. Phys. Lett.* **102**, 032104 (2013).
- [6] T. Hiyoshi and T. Kimoto, Elimination of the major deep levels in n- and p-type 4H-SiC by two-step thermal treatment, *Appl. Phys. Express* **2**, 091101 (2009).
- [7] K. Kawahara, J. Suda, and T. Kimoto, Deep levels generated by thermal oxidation in n-type 4H-SiC, *Appl. Phys. Express* **6**, 051301 (2013).
- [8] B. Zippelius, J. Suda, and T. Kimoto, High temperature annealing of n-type 4H-SiC: Impact on intrinsic defects and carrier lifetime, *J. Appl. Phys.* **111**, 033515 (2012).
- [9] K. Kawahara, J. Suda, and T. Kimoto, Deep levels generated by thermal oxidation in p-type 4H-SiC, *J. Appl. Phys.* **113**, 033705 (2013).
- [10] T. Okuda, G. Alfieri, T. Kimoto, and J. Suda, Oxidation-induced majority and minority carrier traps in n-and p-type 4H-SiC, *Appl. Phys. Express* **8**, 111301 (2015).
- [11] K. Kawahara, J. Suda, and T. Kimoto, Analytical model for reduction of deep levels in SiC by thermal oxidation, *J. Appl. Phys.* **111**, 053710 (2012).
- [12] O. Kordina, C. Hallin, A. Henry, J. P. Bergman, I. Ivanov, A. Ellison, N. T. Son, and E. Janzén, Growth of SiC by "Hot-wall" CVD and HTCVD, *Phys. Status Solidi B* **202**, 321 (1997).
- [13] D. V. Lang, Deep level transient spectroscopy: A new method to characterize traps in semiconductors, *J. Appl. Phys.* **45**, 3023 (1974).
- [14] H. Lefèvre and M. Schulz, Double correlation technique (DDLTS) for the analysis of deep level profiles in semiconductors, *Appl. Phys.* **12**, 45 (1977).
- [15] G. P. Li and K. L. Wang, The use of spatially-dependent carrier capture rates for deep-level-defect transient studies, *Solid State Electron.* **26**, 825 (1983).
- [16] R. Brunwin, B. Hamilton, P. Jordan, and A. R. Peaker, Detection of minority-carrier traps using transient spectroscopy, *Electron. Lett.* **15**, 349 (1979).
- [17] E. F. Ferrari, M. Koehler, and I. A. Hümmelgen, Capacitance-transient-spectroscopy model for defects with two charge states, *Phys. Rev. B* **55**, 9590 (1997).
- [18] A. A. Istratov, New correlation procedure for the improvement of resolution of deep level transient spectroscopy of semiconductors, *J. Appl. Phys.* **82**, 2965 (1997).
- [19] O. Engström and A. Alm, Thermodynamical analysis of optimal recombination centers in thyristors, *Solid State Electron.* **21**, 1571 (1978).
- [20] P. Blood and W. Orton, *The Electrical Characterization of Semiconductors: Majority Carriers and Electron States* (Academic Press, London, 1992).
- [21] C. H. Henry and D. V. Lang, Nonradiative capture and recombination by multiphonon emission in GaAs and GaP, *Phys. Rev. B* **15**, 989 (1977).
- [22] R. M. Gibb, G. J. Rees, B. W. Thomas, B. L. H. Wilson, B. Hamilton, D. R. Wight, and N. F. Mott, A two stage model for deep level capture, *Philos. Mag.* **36**, 1021 (1977).
- [23] P. B. Klein, Carrier lifetime measurement in n- 4H-SiC epilayers, *J. Appl. Phys.* **103**, 033702 (2008).
- [24] I. D. Booker, H. Abdalla, L. Lilja, J. Hassan, J. P. Bergman, E. Ö. Sveinbjörnsson, and E. Janzén, Oxidation induced ON1, ON2_{a/b} defects in 4H-SiC characterized by DLTS, *Mater. Sci. Forum* **778–780**, 281 (2014).
- [25] N. T. Son, X. T. Trinh, L. S. Løvlie, B. G. Svensson, K. Kawahara, J. Suda, T. Kimoto, T. Umeda, J. Isoya, T. Makino, T. Ohshima, and E. Janzén, Negative-*U* System of Carbon Vacancy in 4H-SiC, *Phys. Rev. Lett.* **109**, 187603 (2012).
- [26] I. D. Booker, E. Janzén, N. T. Son, J. Hassan, M. Yazdanfar, P. Stenberg, T. Ohshima, and E. Ö. Sveinbjörnsson (to be published).
- [27] W. R. Buchwald, H. G. Grimmeiss, F. C. Rong, N. M. Johnson, E. H. Poindexter, and H. Pettersson, A reevaluation of electric-field enhanced emission measurements for use in type and charge state determination of point defects, *Mater. Sci. Forum* **83–87**, 1153 (1992).
- [28] G. Alfieri and T. Kimoto, Resolving the EH_{6/7} level in 4H-SiC by Laplace-transform deep level transient spectroscopy, *Appl. Phys. Lett.* **102**, 152108 (2013).
- [29] I. D. Booker, J. Hassan, L. Lilja, F. C. Beyer, R. Karhu, J. P. Bergman, Ö. Danielsson, O. Kordina, E. Ö. Sveinbjörnsson, and E. Janzén, Carrier lifetime controlling defects Z_{1/2} and RB1 in standard and chlorinated chemistry grown 4H-SiC, *Cryst. Growth Des.* **14**, 4104 (2014).
- [30] T. Miyazawa and H. Tsuchida, Point defect reduction and carrier lifetime improvement of Si- and C-face 4H-SiC epilayers, *J. Appl. Phys.* **113**, 083714 (2013).
- [31] S. Ichikawa, K. Kawahara, J. Suda, and T. Kimoto, Carrier recombination in n-type 4H-SiC epilayers with long carrier lifetimes, *Appl. Phys. Express* **5**, 101301 (2012).
- [32] T. Hayashi, T. Okuda, J. Suda, and T. Kimoto, Decay curve analyses in carrier lifetime measurements of p- and n-type 4H-SiC epilayers, *Jpn. J. Appl. Phys.* **53**, 111301 (2014).
- [33] T. Okuda, T. Miyazawa, H. Tsuchida, T. Kimoto, and J. Suda, Enhancement of carrier lifetime in lightly Al-doped p-type 4H-SiC epitaxial layers by combination of thermal oxidation and hydrogen annealing, *Appl. Phys. Express* **7**, 085501 (2014).
- [34] L. Storasta and H. Tsuchida, Reduction of traps and improvement of carrier lifetime in 4H-SiC epilayers by ion implantation, *Appl. Phys. Lett.* **90**, 062116 (2007).
- [35] A. Gali, P. Deák, P. Ordejón, N. T. Son, E. Janzén, and W. J. Choyke, Aggregation of carbon interstitials in silicon carbide: A theoretical study, *Phys. Rev. B* **68**, 125201 (2003).